scientific reports

Check for updates

OPEN

Regulating the expression of matrix metalloproteinases to inhibit ovarian carcinoma using isoquinoline alkaloid from *Allium ascalonicum*

Karunya Jenin Ravindranath & Hemalatha Srinivasan

Ovarian carcinoma is one of the fatal gynecological cancers due to the lack of clinical symptoms at earlier stages of disease leading to metastasis and lower survival rates. Hence, an in-depth exploration of the mechanisms of metastasis facilitates the development of novel-targeted therapeutic strategies to treat the disease. Research studies have reported that three predominant Matrix metalloproteinases (MMPs), namely, MMP14, MMP2 and MMP9 can induce the migration of ovarian cancer cells, Epithelial-Mesenchymal transition, breakdown of extracellular matrix, upregulation of expression of transcription factors etc. in the microenvironment of ovarian tumors. In our current research, these predominant MMPs were used as target proteins and docked with potential anti-cancerous phyto-nutraceuticals present in *Allium ascalonicum* species. *Allium ascalonicum*, commonly referred to as Shallots is being used in various cuisines worldwide and is still largely unexploited for its anti-cancer properties. Docking results, revealed three potential phyto-nutraceuticals, of which, 1-[[3,5-bis(phenylmethoxy)phenyl]methyl]-6-methoxy-2-methyl-3,4-dihydro-1*H*-isoquinoline, an isoquinoline alkaloid was considered the best, since it exhibits significant binding affinity when compared to that of the standard drug, Melphalan. Molecular dynamic simulation studies exhibited that MMP2 is highly flexible and can form more stable interactions. Furthermore, simulation studies of finest interaction pose of the target MMPs with the best phyto-nutraceutical, revealed stable interactions and occurrence of conformational changes. The results, also suggested that, the best phyto-nutraceutical of *Allium ascalonicum* is a novel isoquinoline alkaloid, with favorable bioavailability scores that interact with target MMPs to control the progression and metastasis of ovarian cancer, proposing the prospect of formulating it into sustainable medications for treating metastasized Ovarian Cancer.

Keywords Ovarian carcinoma, Metastasis, Matrix metalloproteinases, *Allium ascalonicum*, Isoquinoline alkaloid, Molecular dynamic simulation

Abbreviations

OvCa	Ovarian carcinoma
MMPs	Matrix metalloproteinases
ECM	Extracellular matrix
MMP14	Matrix metalloproteinase 14
MT1-MMP	Membrane type-1 matrix metalloproteinase
MMP2	Matrix metalloproteinase 2
TIMP2	Tissue Inhibitor of Metalloproteinase 2
VN	Vitronectin
FN	Fibronectin
MMP9	Matrix metalloproteinase 2
TGF-β	Transforming growth factor-β

School of Life Sciences, B. S. Abdur Rahman Crescent Institute of Science & Technology, Vandalur, Chennai 600048, India. ✉email: hemalatha.sls@bsauniv.ac.in

EMT	Epithelial-mesenchymal transition
GC-MS	Gas chromatography-mass spectrometry
ADME	Absorption, distribution, metabolism, excretion
SDF	Structure data files
PDB	Protein data bank
CSV	Comma-separated files
RMSD	Root mean square deviation
RMSF	Root mean square fluctuation
RNG	Random number generation
HIF-1α	Hypoxia-inducible factor 1-alpha
ER-Positive	Estrogen-receptor postive breast cancer
MAP Kinase	Mitogen activated protein kinase
AKT	Protein Kinase B
PHE	Phenylalanine
LEU	Leucine
SER	Serine
TYR	Tyrosine
CYS	Cysteine
TRP	Tryptophan
PRO	Proline
HIS	Histidine
GLN	Glutamine
ARG	Arginine
ILE	Isoleucine
MET	Methionine
THR	Threonine
ASN	Asparagine
LYS	Lysine
VAL	Valine
ALA	Alanine
ASP	Aspartate
GLU	Glutamate
GLY	Glycine

Ovarian carcinoma (OvCa) is a lethal gynecological disorder with a very low, overall five-year survival rate of 48.8%, majorly due to the absence of apparent medical symptoms during the initial stages of metastasis of the affected patients[1]. Hence, a clear understanding of the mechanisms behind the metastasis of OvCa would facilitate the development of novel therapeutic strategies. One such factor involved in the metastasis of OvCa is the contribution of matrix metalloproteinases (MMPs) in the severity of OvCa[2]. MMPs are a type of proteases that play a crucial role in the tumorigenesis and metastasis of OvCa through the processes of migration, invasion and remodeling of extracellular matrix (ECM) promoting inflammation and angiogenesis[3]. MMP protease family includes nearly 25 zinc-dependent enzymes involved in the catabolism of various ECM proteins, namely, caseins, collagens, elastins and gelatin facilitating progression of cancer and metastasis[4,5]. Studies have reported that metastatic mechanism in OvCa is very distinct as cells exfoliate individually or as multicellular aggregates in the peritoneal cavity, existence of viable matrix-detached cells in ascites fluid followed by adherence to mesothelial lining of abdominal organs are aided by MMPs in the early stages of propagation[6–8].

In our research work, we have focused on three key MMPs, namely, MMP14, MMP2 and MMP9 that were found to be specifically overexpressed in metastasized OvCa cells, each with distinct functionalities[2]. MMP14 also referred as Membrane type-1 matrix metalloproteinase (MT1-MMP) is one of the crucial enzymes that regulate the metastasis of OvCa. An increased expression of MMP14 was observed in OvCa cells when compared with that of benign tumors and normal ovarian tissues resulting in metastatic progression and indigent patient prognosis. Pro-MMP2 is activated by TIMP2 (Tissue Inhibitor of Metalloproteinase 2) in association with MMP14. Subsequently, β1 integrin signaling modulates MMP14 and MMP2 which influences matrix remodeling through cell-matrix contact[2,9,10].

Proteolytic fragments with very high adhesive properties are generated by cleavage of vitronectin (VN) and fibronectin (FN) via. MMP2 as catalyst. Research studies have reported that these proteolytic fragments also play a major role in initiating metastasis through adhesion between mesothelial and tumor cell[2,11,12].

MMP9 is specific for FN and type IV collagen[13]. FN is cleaved by MMP9 resulting in release of active TGF-β (Transforming Growth Factor-β) further facilitating epithelial-mesenchymal transition (EMT)[2,14]. Transcription of MMPs is induced by TGF-β through upregulation of transcription factors.

In this in silico study, Melphalan is used as a standard ligand for comparison of the level of interaction between phyto-nutraceuticals of *A. ascalonicum* and target MMPs in molecular docking. Melphalan, belongs to a group of nitrogen mustard alkylating agents and mainly suggested for the treatment of multiple myeloma[15]. It is also known to exhibit anti-carcinogenic activity in a broader spectrum as is observed in breast and ovarian cancer. It's mode of action involves addition of alkyl groups to the proliferating DNA and inter-linking DNA strands, eventually resulting in inhibition of transcription and ultimately cell death[15]. Administration of Melphalan to ovarian cancer patients were reported to produce side-effects such as myelosuppression, diarrhea, mucositis[16] and drug-resistance[15]. Overcoming these side-effects using natural resources will have long-term benefits for the well-being of the patients afflicted with the disease.

In this study, anti-cancerous phytocompounds obtained from Gas-Chromatography Mass Spectrometry (GC-MS) analysis of *Allium ascalonicum* were used, as they have already been proven to possess anti-carcinogenic activity through in silico and in vitro (using MCF-7 cell lines)[17] approaches in breast cancer. Hence, we would like to explore if the same anti-cancerous phyto-nutraceuticals possess anti-carcinogenic activity against ovarian cancer through molecular docking, dynamics and simulation study.

Methods

Virtual screening of anti-carcinogenic phyto-nutraceuticals

Anti-carcinogenic phyto-nutraceuticals of *Allium ascalonicum* previously identified in the research work, nearly 13 of them[17] were used in this study. The common names, IUPAC names and the PubChem ID of the phyto-nutraceuticals used in our study were given in Table 1. Melphalan, a chemotherapeutic drug, used for treating ovarian cancer was used as standard for comparative analysis of binding affinity scores. The anti-carcinogenic phytocompounds and the standard were virtually screened using SwissADME (http://www.swissadme.ch/) to identify if any of them violate "Lipinski's Rule of Five" and also for the determination of pharmacokinetic properties, namely, absorption, distribution, metabolism and excretion (ADME). Phyto-nutraceuticals with number of Lipinski's violations as either 0 or 1 were chosen for the study.

Preparation of anti-carcinogenic phyto-nutraceuticals

The three-dimensional structure of Phyto-nutraceuticals were obtained from PubChem (Fig. 1) (https://pubchem.ncbi.nlm.nih.gov/) as Structure Data Files (SDF format) which were later converted to pdbqt file using a multiple-ligand docking, virtual screening tool, PyRx.

Preparation of target MMPs

The three-dimensional structure of the target matrix metalloproteinases, namely, MMP14, MMP2 and MMP9 that were experimentally determined using X-ray diffraction were downloaded from Protein Data Bank (PDB) website, https://www.rcsb.org/. 3D structure of MMP14, PDB ID being 3C7X (Hemopexin-like domain of MMP14) was obtained from https://www.rcsb.org/structure/3C7X, 3D structure of MMP2, PDB ID being 7XJO (Catalytic domain of MMP2 in complex with inhibitor) was obtained from https://www.rcsb.org/structure/7XJO and 3D structure of MMP9, PDB ID being 1L6J (Human MMP9-gelatinase B) was obtained from (https://www.rcsb.org/structure/1L6J).

Water, heteroatoms and ligands groups were removed from the target MMPs and polar hydrogens were added using BIOVIA Discovery Studio Visualizer 2021 (Fig. 2) (https://discover.3ds.com/discovery-studio-visualizer-download).

Molecular docking

In silico molecular docking of the anti-cancerous phyto-nutraceuticals of *A. ascalonicum* with target MMPs was performed using multi-ligand docking program called PyRx, Version 0.9.9 (https://pyrx.sourceforge.io/, https://pyrx.sourceforge.io/blog) using Autodock Vina-plugin tool[18]. Target MMPs in PDB format were loaded using "Load molecule" option and then converted to macromolecule, resulting in pdbqt formats of target MMPs. SDF format of anti-carcinogenic phyto-nutraceuticals were loaded one by one using "Open Babel" option and then they were prepared by selecting "Minimize all" and "Convert all to pdbqt". Multi-ligand docking program was run using "Vina Wizard" plugin tool where grid dimensions can be adjusted in a way that the whole molecule gets embedded within the grid box to perform global docking[19]. The grid box dimensions of MMP14 were set at X: 62.0742Å, Y: 50.9865Å, Z: 25.000Å and grid center at X:27.7763, Y:9.2125, Z: 4.0364. Similarly, for MMP2, the

S. no.	Common names of phyto-nutraceuticals in "Allium ascalonicum"	IUPAC names	PubChem ID
1.	Melphalan (Standard)	(2*S*)-2-amino-3-[4-[bis(2-chloroethyl)amino]phenyl]propanoic acid	460,612
2.	Benzaldehyde	benzaldehyde	240
3.	Isoquinoline, 1-[3,5-benzyloxybenzyl]-6-methoxy-N-methyl-	1-[[3,5-bis(phenylmethoxy)phenyl]methyl]-6-methoxy-2-methyl-3,4-dihydro-1*H*-isoquinoline	600,532
4.	Succinic acid, diamide, N,N'-diethyl-N, N'-diphenyl-	*N*,*N*'-diethyl-*N*,*N*'-diphenylbutanediamide	1,790,971
5.	N-(4-Bromomethylphenyl)acetamide	*N*-[4-(bromomethyl)phenyl]acetamide	149,290
6.	Octahydropyrrolo[1,2-a]pyrazine	1,2,3,4,6,7,8,8*a*-octahydropyrrolo[1,2-a]pyrazine	558,578
7.	Oxirane, 2,3-dimethyl-, cis-	(2*R*,3*S*)-2,3-dimethyloxirane	92,162
8.	Pyrrole, 2-methyl-5-phenyl-	2-methyl-5-phenyl-1*H*-pyrrole	200,981
9.	2-Amino-4-phenylpyrimidine	4-phenylpyrimidin-2-amine	598,777
10.	2-Fluoro-5-dimethylaminopyrimidine	2-fluoro-*N*,*N*-dimethylpyrimidin-5-amine	587,803
11.	2-Propenal	prop-2-enal	7847
12.	2-Thiophenecarboxaldehyde	thiophene-2-carbaldehyde	7364
13.	6-Indolizinecarbonitrile, 2-methyl-	2-methylindolizine-6-carbonitrile	593,368
14.	6-Methoxy-4-methylquinoline-2-thiol	6-methoxy-4-methyl-1*H*-quinoline-2-thione	935,963

Table 1. IUPAC names and pubchem ID of the potential anti-carcinogenic phyto-nutraceuticals found in *Allium ascalonicum*.

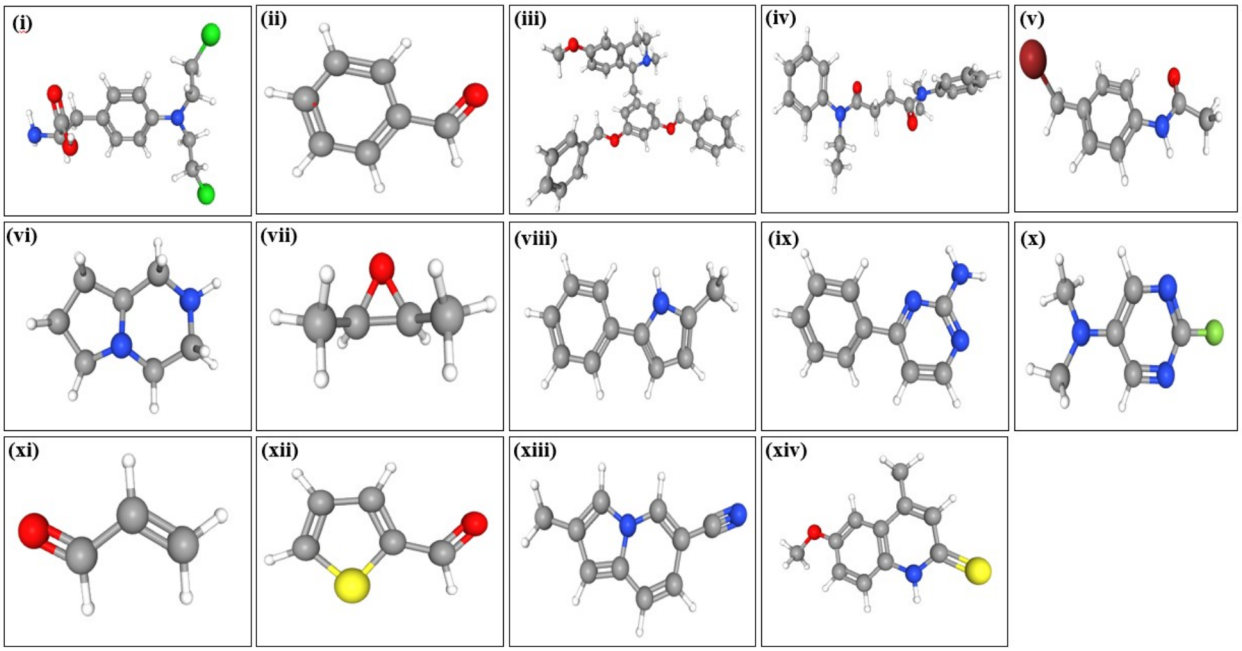

Fig. 1. 3D conformer of Standard and anti-carcinogenic phytocompounds of *Allium ascalonicum*(i) Melphalan-Standard drug ((2*S*)-2-amino-3-[4-[bis(2-chloroethyl)amino]phenyl]propanoic acid) (ii) benzaldehyde (iii) 1-[[3,5-bis(phenylmethoxy)phenyl]methyl]-6-methoxy-2-methyl-3,4-dihydro-1*H*-isoquinoline (iv) *N*,*N*'-diethyl-*N*,*N*'-diphenylbutanediamide (v) *N*-[4-(bromomethyl)phenyl]acetamide (vi) 1,2,3,4,6,7,8,8*a*-octahydropyrrolo[1,2-a]pyrazine (vii) (2*R*,3*S*)-2,3-dimethyloxirane (viii) 2-methyl-5-phenyl-1*H*-pyrrole (ix) 4-phenylpyrimidin-2-amine (x) 2-fluoro-*N*,*N*-dimethylpyrimidin-5-amine (xi) prop-2-enal (xii) thiophene-2-carbaldehyde (xiii) 2-methylindolizine-6-carbonitrile and (xiv) 6-methoxy-4-methyl-1*H*-quinoline-2-thione as obtained in PubChem.

Fig. 2

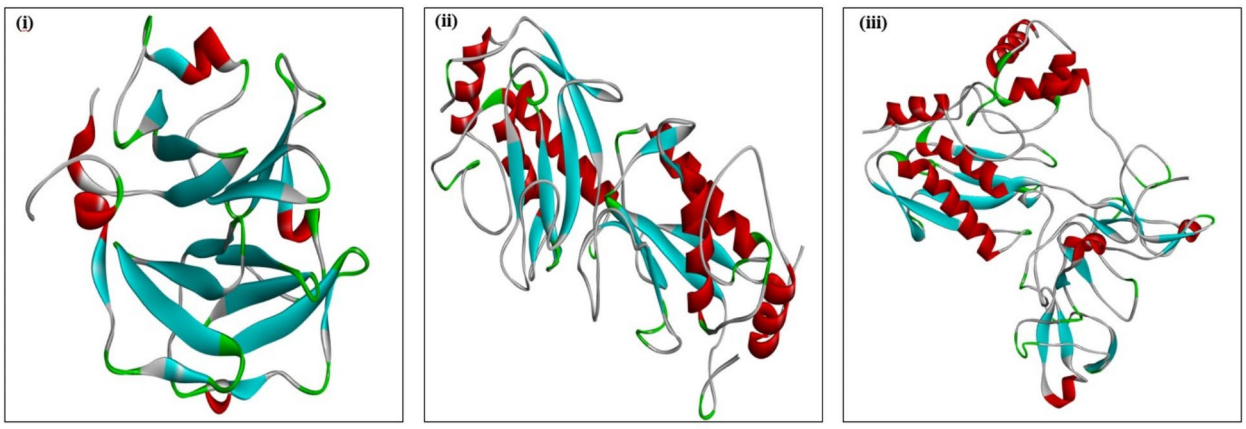

Fig. 2. 3D structure of target MMPs prepared in BIOVIA discovery studio visualizer 2021. (i) MMP14, (ii) MMP2 and (iii) MMP9.

grid box was set at X: 78.3367Å, Y: 64.0885Å, Z: 25.000Å and grid center at X: 44.5846, Y: -46.1620, Z :9.2002. Finally, for MMP9, the grid box was set at X: 67.7970Å, Y: 75.6484Å, Z: 67.7970Å and grid center at X: 36.8831, Y: 34.8814, Z :34.5758. Molecular docking was then run and the status of the docking can be viewed in the bottom panel of PyRx screen.

On completion, binding affinity scores of all the phyto-nutraceuticals under study with that of the target MMP were obtained as comma-separated values (CSV) file and can be viewed using Microsoft Excel program. Phyto-nutraceuticals with binding affinity scores greater than or equal to -6Kcal/mol with RMSD and RMSF

values 0 were chosen for further analysis. The same procedure was repeated for each of the target MMPs under study.

Determination of 2D interactions between target MMPs and anti-carcinogenic phyto-nutraceuticals

2D interaction images were obtained by viewing them in BIOVIA Discovery Studio Visualizer 2021. The best docking model-run of the anti-carcinogenic phyto-nutraceuticals with that of the target MMPs (obtained in PyRx) under study were saved in PDB format and then subsequently viewed in BIOVIA Discovery Studio Visualizer. The images of the best model-run and the target MMPs were viewed and the "Hierarchy" option under the view tab was chosen. The images were superimposed by copying the hierarchy of the phyto-nutraceutical and pasting it onto the protein hierarchy. On selecting, "Ligand interactions" the specific position at which the phyto-nutraceutical interacts with that of the target MMPs was highlighted in the form of circles in fluorescent green colour. The two-dimensional interaction images (obtained by selecting "Show 2D diagram") gives us information about the specific amino acid residues of the target MMPs which interact with that of anti-carcinogenic phyto-nutraceuticals.

Molecular dynamics of target MMPs using simulation

Molecular dynamics and simulation studies gives us a deeper insight into the stability and the flexibility of target proteins and its interaction with ligands. It also helps us to virtually predict the conformational changes that would have occurred in the target proteins after binding of ligands. Molecular dynamics was simulated using CABS-flex 2.0, (http://biocomp.chem.uw.edu.pl/CABSflex2) a coarse-grained protein model that acts a protein engine[20] to determine the flexibility of target MMPs. The PDB code or the PDB file of the target MMPs were given as input and then submitted by selecting the chain/chains of target MMPs that needs to be analysed along with the project name and e-mail address (for obtaining the link for output). Additional and advanced parameters in the simulation were kept as default. However, they can also be changed according to user's requirements. Simulation was then run for each one of the target MMPs individually.

Comparative analysis of Simulation between individual MMPs and finest interaction pose of MMPs with the best ligand

The best ligand from the molecular docking studies was chosen and a comparative simulation analysis was performed between the individual target MMPs and the finest interaction pose of MMPs with the best ligand to determine the specific position/location of stable interactions with the help of 2D fluctuation plots. Conformational changes in the target proteins were also be determined by superimposing the best simulation models (model-1) obtained using CABS-flex 2.0 server.

Results and discussion

Drug-likeness and Pharmacokinetic analysis of anti-carcinogenic phyto-nutraceuticals

Drug likeness of anti-carcinogenic phyto-nutraceuticals of *Allium ascalonicum* were determined using Lipinski's rule of five (Table 2) and it was observed that all of the anti-carcinogenic phytocompounds obeyed Rule of Five, except 1-[[3,5-bis(phenylmethoxy)phenyl]methyl]-6-methoxy-2-methyl-3,4-dihydro-1*H*-isoquinoline having a minimal number of Lipinski's violations (1-acceptable value). Pharmacokinetic properties such as Absorption, Distribution, Metabolism and Excretion (ADME) including bioavailability of the anti-carcinogenic phyto-nutraceuticals were determined using SwissADME and are listed in Table 3. It was observed that most of the anti-carcinogenic phyto-nutraceuticals possess very high GI absorption and have a higher bioavailability score

S.No	Anti-carcinogenic phyto-nutraceuticals	Molecular Weight (g/mol)	#H-bond acceptors	#H-bond donors	Consensus Log *P*	Molar refractivity	#Lipinski violations
1.	Melphalan (Standard)	305.20	3	2	1.31	78.91	0
2.	benzaldehyde	106.12	1	0	1.57	31.83	0
3.	1-[[3,5-bis(phenylmethoxy)phenyl]methyl]-6-methoxy-2-methyl-3,4-dihydro-1*H*-isoquinoline	479.61	4	0	5.78	148.43	1
4.	*N*,*N*'-diethyl-*N*,*N*'-diphenylbutanediamide	324.42	2	0	3.34	98.81	0
5.	*N*-[4-(bromomethyl)phenyl]acetamide	228.09	1	1	2.15	53.59	0
6.	1,2,3,4,6,7,8,8*a*-octahydropyrrolo[1,2-a]pyrazine	126.2	2	1	0.57	45.06	0
7.	(2*R*,3*S*)-2,3-dimethyloxirane	72.11	1	0	0.99	20.31	0
8.	2-methyl-5-phenyl-1*H*-pyrrole	157.21	0	1	2.73	51.19	0
9.	4-phenylpyrimidin-2-amine	171.2	2	1	1.55	51.87	0
10.	2-fluoro-*N*,*N*-dimethylpyrimidin-5-amine	141.15	3	0	0.91	36.20	0
11.	prop-2-enal	56.06	1	0	0.35	16.26	0
12.	thiophene-2-carbaldehyde	112.15	1	0	1.42	29.71	0
13.	2-methylindolizine-6-carbonitrile	156.18	1	0	1.98	47.08	0
14.	6-methoxy-4-methyl-1*H*-quinoline-2-thione	205.28	1	1	2.72	60.59	0

Table 2. Drug likeness of anti-carcinogenic phyto-nutraceuticals of *Allium ascalonicum*.

S.no	Anti-carcinogenic phyto-nutraceuticals	Water solubility Log S (ESOL)	GI Absorption	BBB permeant	*P*-gp substrate	Skin permeation (Log K_p) (in cm/sec)	Bioavailability score
1.	Melphalan (Standard)	-1.56	High	Yes	No	-8.02	0.55
2.	Benzaldehyde	-1.92	High	Yes	No	-5.90	0.55
3.	1-[[3,5-bis(phenylmethoxy)phenyl]methyl]-6-methoxy-2-methyl-3,4-dihydro-1*H*-isoquinoline	-6.92	High	Yes	Yes	-4.48	0.55
4.	*N*,*N*'-diethyl-*N*,*N*'-diphenylbutanediamide	-3.48	High	Yes	No	-6.19	0.55
5.	*N*-[4-(bromomethyl)phenyl]acetamide	-2.62	High	Yes	No	-6.35	0.55
6.	1,2,3,4,6,7,8,8*a*-octahydropyrrolo[1,2-a]pyrazine	-0.72	Low	No	No	-6.96	0.55
7.	(2*R*,3*S*)-2,3-dimethyloxirane	-0.74	Low	No	No	-6.23	0.55
8.	2-methyl-5-phenyl-1*H*-pyrrole	-3.17	High	Yes	No	-5.29	0.55
9.	4-phenylpyrimidin-2-amine	-2.48	High	Yes	No	-6.27	0.55
10.	2-fluoro-*N*,*N*-dimethylpyrimidin-5-amine	-1.57	High	Yes	No	-6.62	0.55
11.	prop-2-enal	-0.12	Low	No	No	-6.65	0.55
12.	thiophene-2-carbaldehyde	-1.64	High	Yes	No	-6.26	0.55
13.	2-methylindolizine-6-carbonitrile	-2.99	High	Yes	No	-5.42	0.55
14.	6-methoxy-4-methyl-1*H*-quinoline-2-thione	-2.72	High	Yes	No	-6.26	0.55

Table 3. Pharmacokinetic analysis of anti-carcinogenic phyto-nutraceuticals of *Allium ascalonicum*.

S. no.	Best Ligands	Binding Affinity (Kcal/mol) Target Protein: MMP14	Binding Affinity (Kcal/mol) Target Protein: MMP2	Binding Affinity (Kcal/mol) Target Protein: MMP9
Standard	Melphalan	-5.1	-7.2	-5.2
1.	1-[[3,5-bis(phenylmethoxy)phenyl]methyl]-6-methoxy-2-methyl-3,4-dihydro-1*H*-isoquinoline	***-7***	***-9.9***	***-8.5***
2.	4-phenylpyrimidin-2-amine	***-6***	***-8***	***-8***
3.	2-methyl-5-phenyl-1*H*-pyrrole	***-6***	***-7.3***	***-7.5***
4.	2-methylindolizine-6-carbonitrile	-5.9	***-7.2***	***-7.6***
5.	*N*,*N*'-diethyl-*N*,*N*'-diphenylbutanediamide	***-6.2***	-7	***-6***
6.	*N*-[4-(bromomethyl)phenyl]acetamide	-5.6	-6.9	***-6.8***
7.	6-methoxy-4-methyl-1*H*-quinoline-2-thione	-5.5	-6.2	***-6.1***

Table 4. Potential anti-carcinogenic phyto-nutraceuticals ranked based on binding affinity scores. *Italicized binding affinity values represent potential phytonutraceuticals having comparatively higher binding affinity scores than that of the Standard drug, Melphalan.

of 0.55, suggesting active drug-like characteristics and are more suitable for consumption as oral drugs[21,22]. It was also observed that majority of the anti-carcinogenic phyto-nutraceuticals have a higher negative value for Log Kp, lesser than − 6, indicating lower chances of permeation through the skin[23].

Molecular docking analysis

Molecular docking was performed between the anti-carcinogenic phyto-nutraceuticals of *Allium ascalonicum* with three target MMPs, namely, MMP14, MMP2 and MMP9 using PyRx, version 0.9.9. Anti-carcinogenic phyto-nutraceuticals that had comparatively better binding affinity scores than the standard drug, Melphalan were analysed and ranked accordingly (Table 4). Two-dimensional interactions of the ranked phyto-nutraceuticals along with details about specific aminoacid residues involved were determined and represented in Figs. 3, 4 and 5. Furthermore, the details of the specific amino acid interactions were also listed out in Table 5. 1-[[3,5-bis(phenylmethoxy)phenyl]methyl]-6-methoxy-2-methyl-3,4-dihydro-1*H*-isoquinoline; *N*,*N*'-diethyl-*N*,*N*'-diphenylbutanediamide and 2-methyl-5-phenyl-1*H*-pyrrole represented the top three potential anti-carcinogenic phyto-nutraceuticals against ovarian cancer progression. However, 1-[[3,5-bis(phenylmethoxy) phenyl]methyl]-6-methoxy-2-methyl-3,4-dihydro-1*H*-isoquinoline can be considered as the best anti-carcinogenic phyto-nutraceutical present in *A. Ascalonicum* as it targets all the three MMPs; MMP14, MMP2 and MMP9 very efficiently with binding affinity scores of -7Kcal/mol, -9.9Kcal/mol and − 8.5Kcal/mol respectively.

Analysis of molecular dynamics of target MMPs using simulation

Molecular dynamics of the target MMPs were determined using CABS-flex 2.0 server. It is one of the user-friendliest computational tools for studying molecular dynamics. The software has an embedded simulation engine that can efficiently model even large-scale protein systems with various conformational transitions[20]. The webpage containing the simulation results has four distinct sections. The first section has complete project

Fig. 3

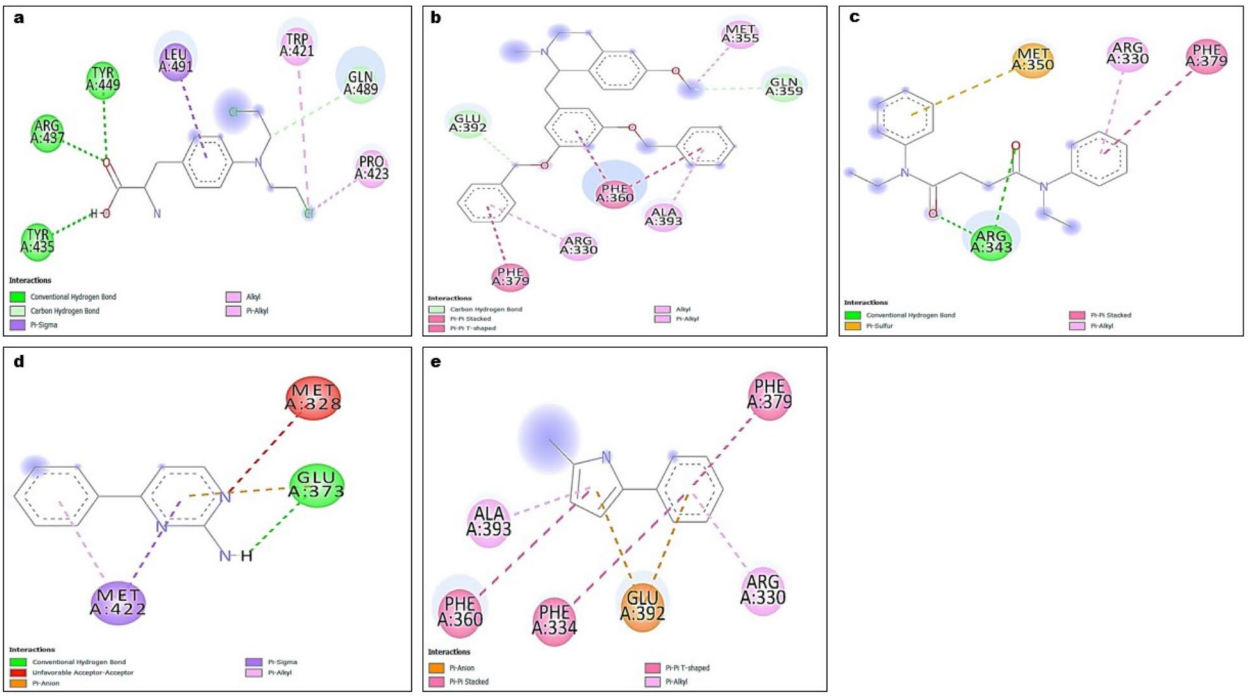

Fig. 3. 2D Interaction images of MMP14 with the standard and the best phytonutraceuticals. (a) Melphalan **(b)** 1-[[3,5-bis(phenylmethoxy)phenyl]methyl]-6-methoxy-2-methyl-3,4-dihydro-1*H*-isoquinoline **(c)***N*,*N*'-diethyl-*N*,*N*'-diphenylbutanediamide **(d)** 4-phenylpyrimidin-2-amine **(e)** 2-methyl-5-phenyl-1*H*-pyrrole.

Fig. 4

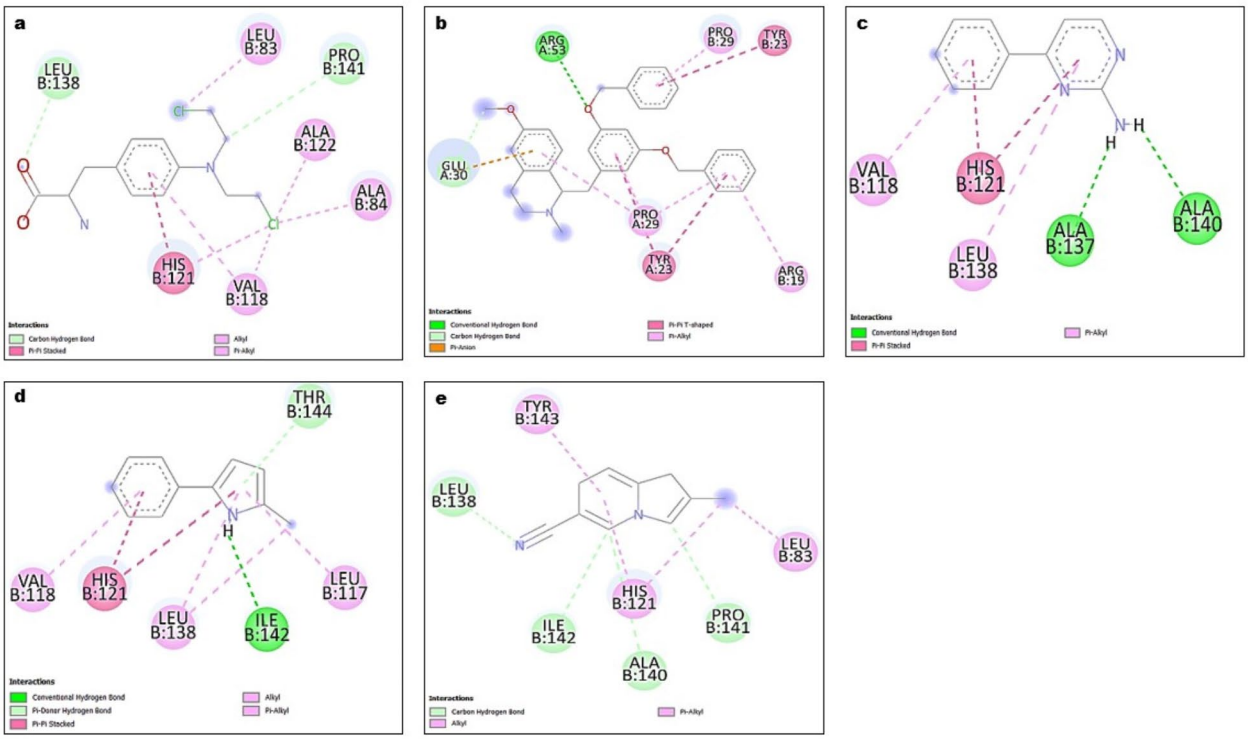

Fig. 4. 2D Interaction images of MMP2 with the standard and the best phytonutraceuticals. (a) Melphalan **(b)** 1-[[3,5-bis(phenylmethoxy)phenyl]methyl]-6-methoxy-2-methyl-3,4-dihydro-1*H*-isoquinoline **(c)** 4-phenylpyrimidin-2-amine **(d)** 2-methyl-5-phenyl-1*H*-pyrrole **(e)** 2-methylindolizine-6-carbonitrile.

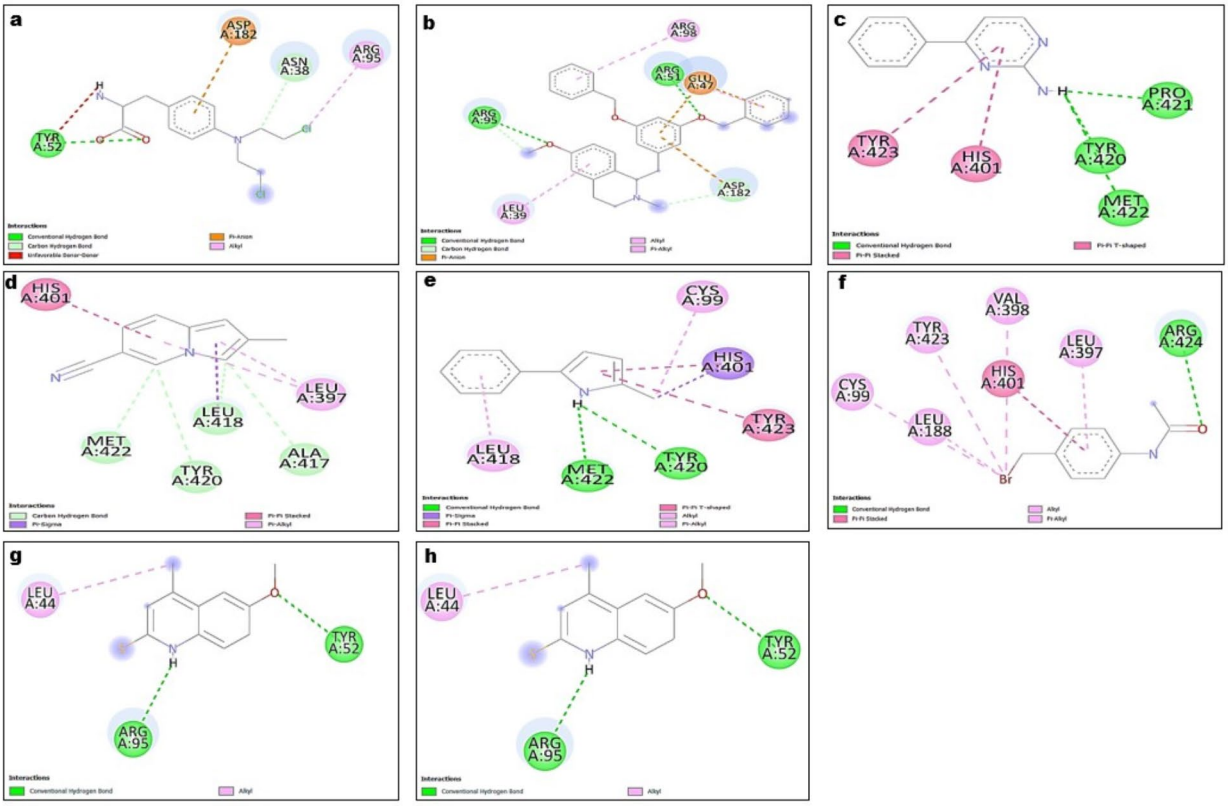

Fig. 5. 2D Interaction images of MMP9 with the standard and the best phytonutraceuticals. (a) Melphalan **(b)** 1-[[3,5-bis(phenylmethoxy)phenyl]methyl]-6-methoxy-2-methyl-3,4-dihydro-1*H*-isoquinoline **(c)** 4-phenylpyrimidin-2-amine **(d)** 2-methylindolizine-6-carbonitrile **(e)** 2-methyl-5-phenyl-1*H*-pyrrole **(f)***N*-[4-(bromomethyl)phenyl]acetamide **(g)** 6-methoxy-4-methyl-1*H*-quinoline-2-thione **(h)***N*,*N*'-diethyl-*N*,*N*'-diphenylbutanediamide.

Target MMPs	Phyto-nutraceuticals	Interacting Amino acid residues
MMP14	**Melphalan**	**TYR435**, **ARG437**, **TYR449**, **LEU491**, **TRP421**, **GLN489**, **PRO423**
	1-[[3,5-bis(phenylmethoxy)phenyl]methyl]-6-methoxy-2-methyl-3,4-dihydro-1*H*-isoquinoline	GLU392, PHE379, ARG330, PHE360, ALA393, MET355, GLN359
	N,*N*'-diethyl-*N*,*N*'-diphenylbutanediamide	MET350, ARG330, PHE379, ARG343
	4-phenylpyrimidin-2-amine	MET328, GLU373, MET422
	2-methyl-5-phenyl-1*H*-pyrrole	ALA393, PHE360, PHE334, GLU392, ARG330, PHE379
MMP2	**Melphalan**	LEU138, HIS121, VAL118, ALA84, ALA122, LEU83, PRO141
	1-[[3,5-bis(phenylmethoxy)phenyl]methyl]-6-methoxy-2-methyl-3,4-dihydro-1*H*-isoquinoline	ARG53, GLU30, TYR23, PRO29, TYR23, ARG19
	4-phenylpyrimidin-2-amine	VAL118, LEU138, HIS121, ALA137, ALA140
	2-methyl-5-phenyl-1*H*-pyrrole	THR144, VAL118, HIS121, LEU138, ILE142, LEU117
	2-methylindolizine-6-carbonitrile	TYR143, LEU138, ILE142, HIS121, ALA140, PRO141, LEU83
MMP9	**Melphalan**	TYR52, ASP182, ASN38, ARG95
	1-[[3,5-bis(phenylmethoxy)phenyl]methyl]-6-methoxy-2-methyl-3,4-dihydro-1*H*-isoquinoline	ARG95, LEU39, ASP182, GLU47, ARG51, ARG98
	4-phenylpyrimidin-2-amine	TYR423, HIS401, TYR420, MET422, PRO421
	2-methylindolizine-6-carbonitrile	HIS401, MET422, TYR420, LEU418, ALA417, LEU397
	2-methyl-5-phenyl-1*H*-pyrrole	LEU418, MET422, TYR420, TYR423, HIS401, CYS99
	N-[4-(bromomethyl)phenyl]acetamide	CYS99, TYR423, VAL398, LEU188, HIS401, LEU397, ARG424
	6-methoxy-4-methyl-1*H*-quinoline-2-thione	LEU44, ARG95, TYR52
	N,*N*'-diethyl-*N*,*N*'-diphenylbutanediamide	LEU44, ARG95, TYR52

Table 5. Interaction of potential phyto-nutraceuticals with specific aminoacid residues present in target MMPs.

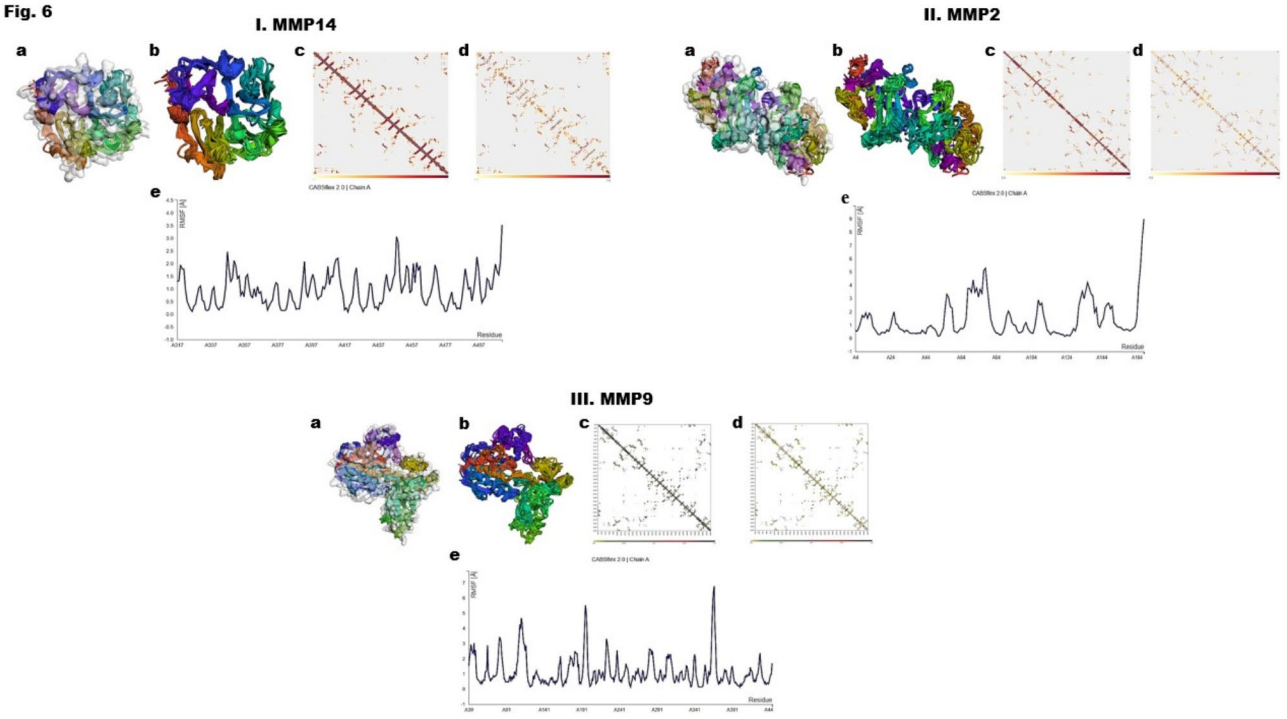

Fig. 6. Molecular dynamics and Simulation studies of target proteins (I) MMP14 **(II)** MMP2 and **(III)** MMP9 where **(a)** Target protein with surface **(b)** Target protein without surface **(c)** Contact Map-Trajectory **(d)** Contact Map-Model all **(e)** 2D Fluctuation Plot.

Target MMPs	RMSF (Å)	Chain	Residue number
MMP14	3.525	A	511
MMP2	***8.9880***	***A***	***168***
MMP9	6.7880	A	367

Table 6. RMSF values for each of the target MMPS along with chain and residue number. *Italicized aminoacid residue-best target MMP as it is more flexible and can form stable interactions.

information in a detailed manner such as restraints (protein, C-alpha distance, Global C-alpha and Global side chain), rigidity, number of cycles and cycles between trajectory and temperature range in which simulation was being carried out. Usually, the above-mentioned parameters were set as default for all the target MMPs under study. However, RNG (Random Number Generation) seed varies between proteins and were found to be 3584, 9140 and 7202 for MMP14, MMP2 and MMP9 respectively. The second section gives us three-dimensional structures of the target MMPs that can be viewed individually or by superimposing images of all the models using the "model-all" option. 3D structures of the target MMPs with or without the molecular surface were also obtained. These can be downloaded and saved as animated files for future reference. The third section, "contact maps" gives information about the different interaction patterns between the aminoacid residues of the target MMPs and are usually represented as dots that are coloured squares. The trajectory maps exhibit the frequency of contacts between the aminoacid residues throughout the period of simulation. The final section is the fluctuation plot where the Root Mean Square Fluctuation (RMSF in Angstorm) were plotted as a 2D graph against each of the aminoacid residues[24] and these are represented in Fig. 6. Table 4 represents the highest RMSF value obtained after simulation for each of the target MMPs along with chain and residue number.

From Table 6, it was observed that MMP2 has the highest RMSF value, followed by MMP9 and MMP14. Hence, molecular dynamics and simulation study of individual target MMPs concluded the fact that MMP2 target protein is more flexible and can form more stable interactions with the anti-carcinogenic phyto-nutraceuticals when compared to that of the other target MMPs.

Molecular dynamics and simulation studies of docked MMPs with the best ligand

The molecular docking studies revealed, 1-[[3,5-bis(phenylmethoxy)phenyl]methyl]-6-methoxy-2-methyl-3,4-dihydro-1*H*-isoquinoline as the best phytonutraceutical as it demonstrated, best binding affinity scores with all the three target MMPs under study. Hence, the finest interaction pose of 1-[[3,5-bis(phenylmethoxy)phenyl]

methyl]-6-methoxy-2-methyl-3,4-dihydro-1*H*-isoquinoline with MMP14, MMP2 and MMP9 were given as input (Fig. 7) in PDB format, in the CABS Flex2.0 sever for further simulation studies[25].

Identification of stable interactions between target MMPs and the best ligand

Comparison of 2D fluctuation plots of MMP14 and finest interaction pose of MMP14 with the best ligand, 1-[[3,5-bis(phenylmethoxy)phenyl]methyl]-6-methoxy-2-methyl-3,4-dihydro-1*H*-isoquinoline revealed two major peaks and few minor peaks as shown (Fig. 8, Table S1). Among the two major peaks, one of them has a higher RMSF value of about 4.277Å at residue GLY511 of Chain A, followed by an other peak atresidue ALA393 with RMSF 3.982Å, higher than the RMSF values at same residue numbers for MMP14 alone. From the fluctuation plots, it can be understood that the binding of 1-[[3,5-bis(phenylmethoxy)phenyl]methyl]-6-methoxy-2-methyl-3,4-dihydro-1*H*-isoquinoline to MMP14 resulted in more flexible and stable interactions at specified amino acid residue numbers.

Similarly, the fluctuation plot of interaction of 1-[[3,5-bis(phenylmethoxy)phenyl]methyl]-6-methoxy-2-methyl-3,4-dihydro-1*H*-isoquinoline with MMP2 demonstrated three major peaks, exhibiting higher RMSF values of 3.873Å at residue TYR55, 4.004Å at residue ASP56 and 3.821Å at residue LYS109 and a few other minor peaks when compared to the RMSF values of same residues of MMP2 alone (Fig. 9, Table S2). It can also be observed from the fluctuation plots, that MMP2 on its own has more number of peaks with higher RMSF values when compared to that of the interaction pose of MMP2 with the best ligand and hence validating the result obtained during simulation of target MMP2 as represented in Table 6. It can also be concluded that binding of 1-[[3,5-bis(phenylmethoxy)phenyl]methyl]-6-methoxy-2-methyl-3,4-dihydro-1*H*-isoquinoline with MMP2 resulted in less stable interactions, in contrary, to the expectation of formation of more stable interactions.

In case of interaction of 1-[[3,5-bis(phenylmethoxy)phenyl]methyl]-6-methoxy-2-methyl-3,4-dihydro-1*H*-isoquinoline with MMP9, fluctuation plots revealed nine major peaks at residues GLY248, ARG249, SER250, ASN341, VAL414, PRO415, GLU416, ALA417 and GLY444 with RMSF values of 3.339Å, 3.152Å, 3.432Å, 5.088Å, 3.874Å, 3.511Å, 2.343Å, 2.509Å and 3.941Å respectively. A large number of minor peaks with higher RMSF values were also observed (Fig. 10, Table S3). Therefore, binding of 1-[[3,5-bis(phenylmethoxy)phenyl]methyl]-6-methoxy-2-methyl-3,4-dihydro-1*H*-isoquinoline to MMP9, resulted in large number of stable interactions (nearly 67), when compared to that of the binding of the best ligand to MMP14 and MMP2. Thus, it can be concluded that MMP9 can form more stable interactions with the best phytonutraceutical of *Allium ascalonicum*, indicating the possibility of targeting a potential protein of therapeutic significance involved in the progression and metastasis of OvCa.

From the finest interaction poses (Fig. 7) and comparison of 2D Fluctuation plots (Figs. 8, 9 and 10), we could infer the presence of few stable interactions between the amino acid residues of the target MMPs with the best ligand as summarized in Table 7.

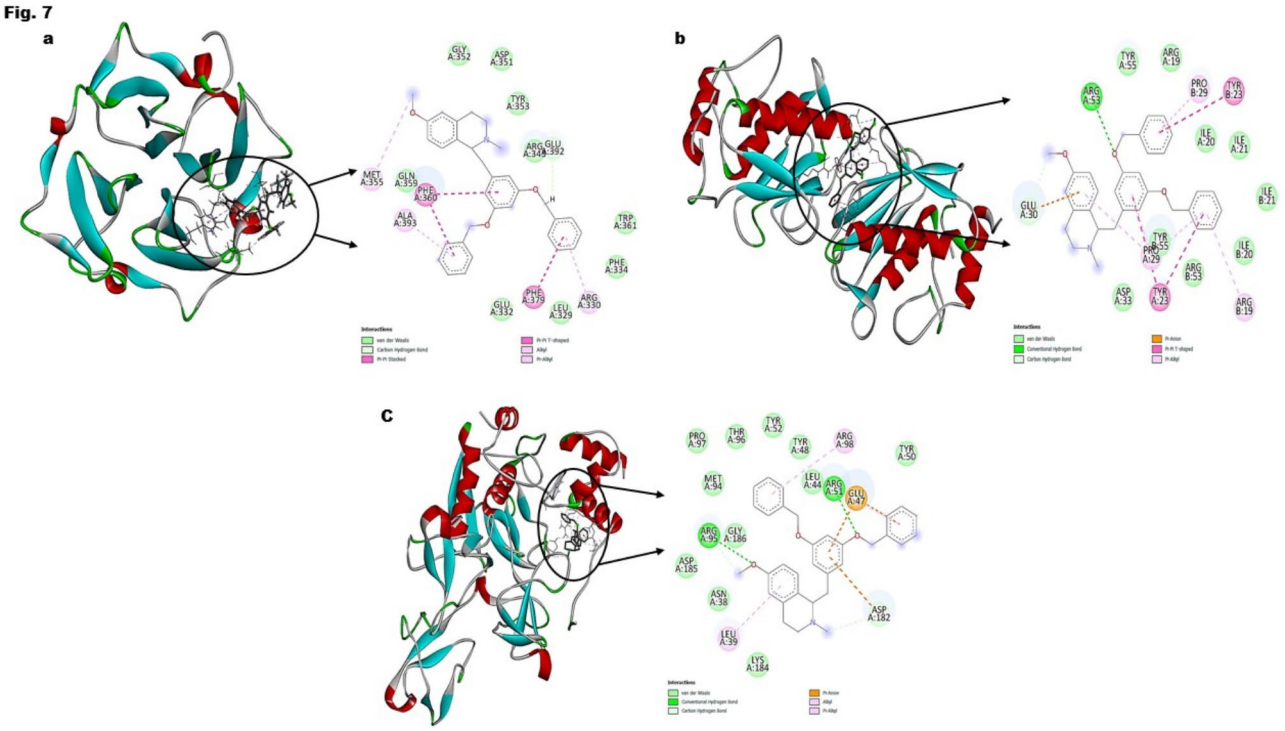

Fig. 7. Finest interaction poses of 1-[[3,5-bis(phenylmethoxy)phenyl]methyl]-6-methoxy-2-methyl-3,4-dihydro-1*H*-isoquinoline with target MMPs (**a**) MMP14, (**b**) MMP2 and (**c**) MMP9.

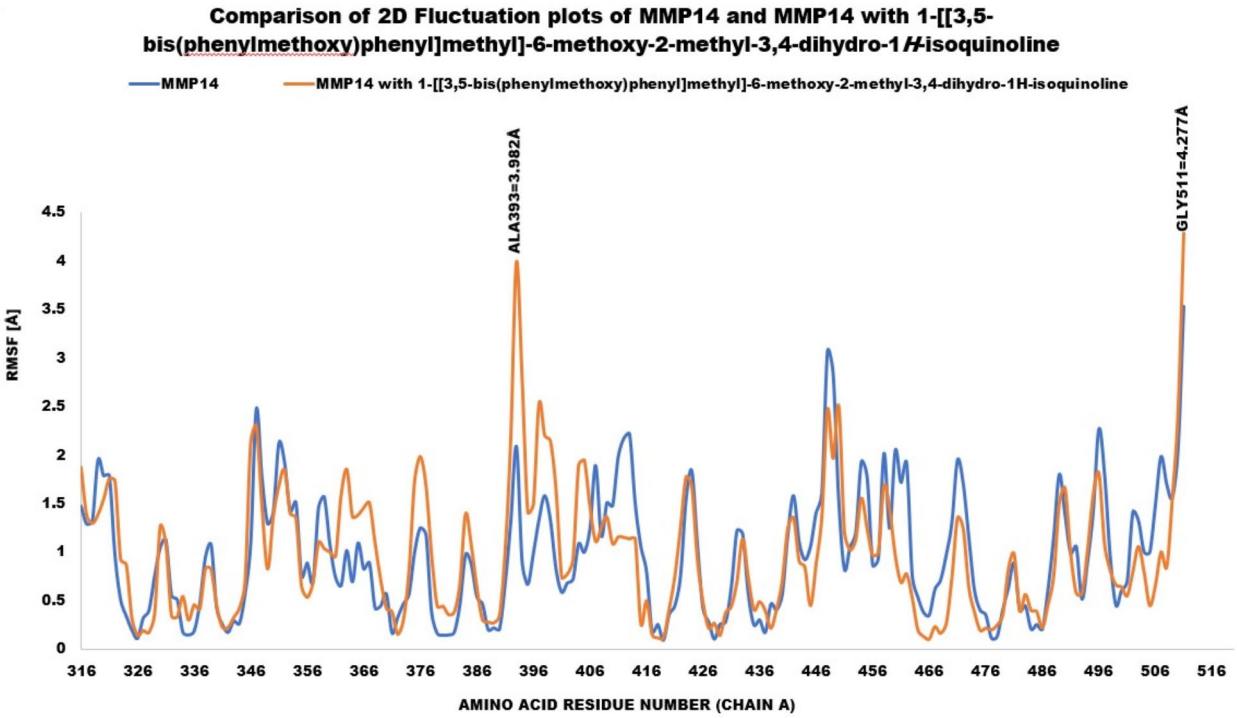

Fig. 8. Comparison of 2D fluctuation plots of MMP14 and MMP14 with 1-[[3,5-bis(phenylmethoxy)phenyl] methyl]-6-methoxy-2-methyl-3,4-dihydro-1*H*-isoquinoline.

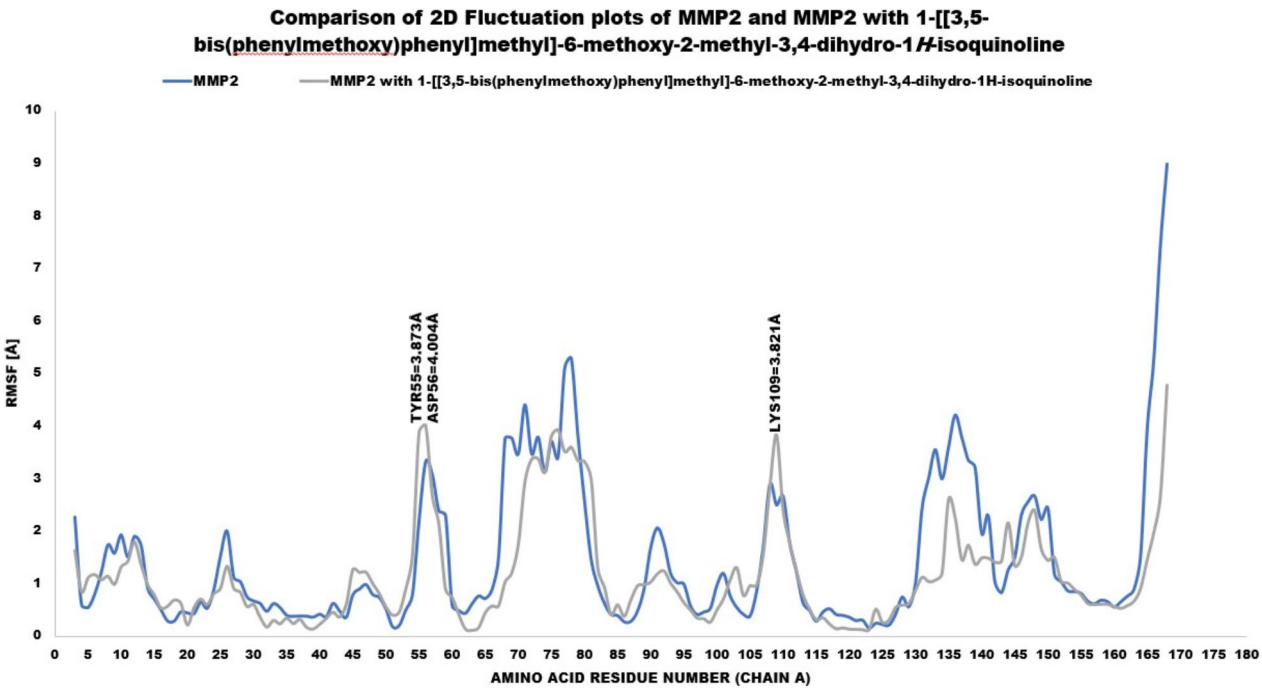

Fig. 9. Comparison of 2D fluctuation plots of MMP2 and MMP2 with 1-[[3,5-bis(phenylmethoxy)phenyl] methyl]-6-methoxy-2-methyl-3,4-dihydro-1*H*-isoquinoline.

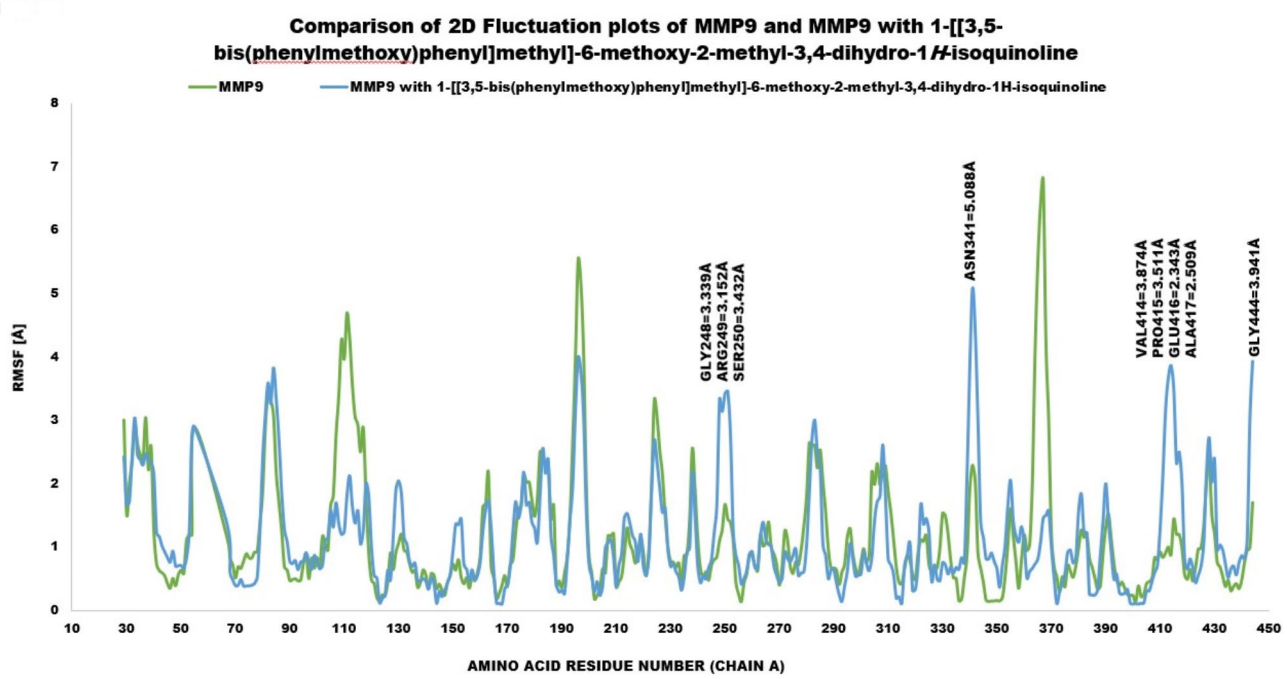

Fig. 10. Comparison of 2D fluctuation plots of MMP9 and MMP9 with 1-[[3,5-bis(phenylmethoxy)phenyl] methyl]-6-methoxy-2-methyl-3,4-dihydro-1*H*-isoquinoline.

Target MMPs	Amino acid residues	Type of interaction
MMP14	ALA393 ARG330	Alkyl Alkyl
MMP2	TYR55	Vander Waal's forces
MMP9	ASP185	Vander Waal's forces

Table 7. Stable interactions determined from the simulation study of the finest interaction poses of the target MMPs with the best ligand.

Identification of conformational changes in the target MMPs after binding with the best ligand

Simulation using CABS Flex 2.0 server, results in 3D models that predict conformational changes in the target proteins after binding with the best ligand. Changes in conformation of the target proteins can be clearly identified by superimposing best models, that is, model 1 of the target protein and model 1 of the finest interaction pose of the target protein with the best ligand. In this study, we represent three superimposed models, namely, MMP14, MMP2 and MMP9 with the best ligand, 1-[[3,5-bis(phenylmethoxy)phenyl]methyl]-6-methoxy-2-methyl-3,4-dihydro-1*H*-isoquinoline (Fig. 11). The distinctly visible differences (secondary structures-amino acid residues) in the 3D models of target MMPs and its interactions with the best ligand were identified and its attributes such as XYZ dimensions of the conformation, Hydrophobicity, pKa, ribbon size, average isotropic displacement and the type of secondary structure formation, such as, helix, turn, sheet and coil were also determined.

On comparison of Fig. 7 with data attributes (refer Tables S4, S5 and S6), we identified few interactions that resulted in conformational changes in the target MMPs on binding with the best ligand (Table 8). Interaction of MMP14 and MMP2 with the best ligand resulted in conformational changes in the 3D structures of target proteins. However, interaction of MMP9 with the target ligand has not resulted in major conformational changes, instead, conformational changes in the other parts of the target MMPs were identified (Table S6).

Impact of naturally occurring Isoquinoline alkaloids and its derivatives on tumor proliferation and EMT through molecular pathways to inhibit metastatic progression of cancer

A study published by Wang[26], demonstrated that the derivatives 1-styrene-isoquinoline inhibited cell cycle progression at G2/M phase facilitating apoptosis, cell migration and invasion by modulating EMT against hepatocellular carcinoma cell lines. The study, further proved that it can hinder the activation of P13K/Akt/mTOR molecular pathway and hence initiating mitochondrial apoptosis pathway. The same study also exhibited tumor-inhibitory effect of 1-styrene-isoquinoline derivatives in the subcutaneous Huh7-xenograft incorporated in nude mice[26].

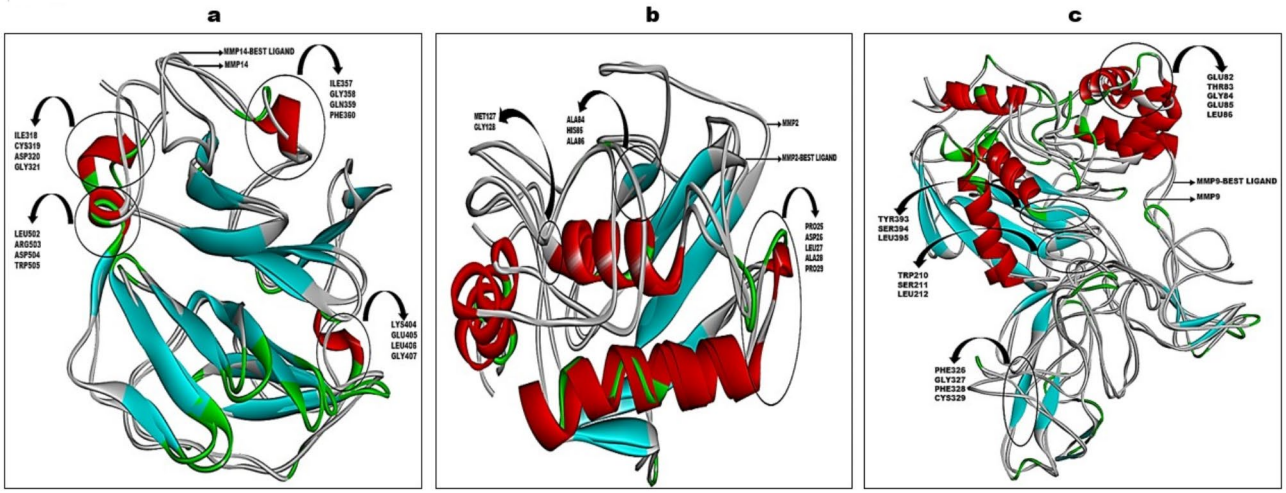

Fig. 11. Superimposed models of the target MMPs and target MMPs with the best ligand (1-[[3,5-bis(phenylmethoxy)phenyl]methyl]-6-methoxy-2-methyl-3,4-dihydro-1*H*-isoquinoline) (**a**) MMP14 (**b**) MMP2 and (**c**) MMP9 for the identification of distinctly visible conformational changes in the secondary structures and the aminoacid residues involved in it.

Target MMPs	Amino acid residues
MMP14	GLN359 PHE360
MMP2	PRO29
MMP9	Nil

Table 8. Conformational changes in the amino acid residues of the target MMPs after binding of best ligand.

Liensinine, an isoquinoline alkaloid, has been reported to interfere with tumor proliferation by arresting cell cycle at G1 phase and EMT transition through, TGF-ß1/P-smad3 molecular signaling pathway via. HIF-1α (Hypoxia-inducible factor 1-alpha) hence preventing the invasion and migration of tumor cells in intrahepatic cholangiocarcinoma. In vivo study of the same compound in nude mice were also found to inhibit the propagation of Hucc-T1 transplanted tumors[27].

Sanguinarine is another isoquinoline alkaloid, which has been exhibited to impede metastasis and inverse EMT transition, post TGF-ß treatment, by inhibiting the cadherin switch in ER-positive breast cancer. It was also found to mask the expression of EMT molecular pathway proteins such as MAP kinase (Mitogen activated Protein Kinase), Smad and P13K/Akt. In vivo studies on bulb/c mice infused with breast cancer cells and then subsequently, treated with Sanguinarine impeded metastatic nodules in the lungs of mice model compared to the untreated mice at the metastatic stage[28].

In vitro and in vivo studies of Isoquinolines and its derivatives have been proven to demonstrate anti-carcinogenic activity against different types of tumors. Hence, in our current research work, 1-[[3,5-bis(phenylmethoxy)phenyl]methyl]-6-methoxy-2-methyl-3,4-dihydro-1*H*-isoquinoline, one of the best phytocompounds of *A. Ascalonicum* with good binding affinity scores and molecular simulation properties, indicate the possibility of the compound playing a vital role in the inhibition of metastatic progression of ovarian cancer. However, studies on anti-cancer activity on cell lines and animal model research work is recommended as future work for confirmation and appropriate formulation for targeted, highly-specific and natural therapy for ovarian cancer.

Conclusion

In silico study on targeting the Matrix Metalloproteinases involved in ovarian cancer progression and metastasis suggests that anti-carcinogenic phytocompounds of *Allium ascalonicum* is effective against ovarian cancer. Pharmacokinetic analysis of the phytocompounds also suggested the fact that they have good bioavailability, suggesting its use as oral drugs. Molecular docking studies identified, 1-[[3,5-bis(phenylmethoxy)phenyl]methyl]-6-methoxy-2-methyl-3,4-dihydro-1*H*-isoquinoline as one of the best phytocompounds of *A. ascalonicum* with good binding affinity scores for all the three target MMPs. A few phytocompounds have also been proved to have comparatively better binding scores than the standard, Melphalan and hence suggesting a good alternative for commercially available chemotherapeutic drug in treating the disease. Moreover, molecular dynamics and simulation studies demonstrated the formation of stable interactions and also indicated the flexibility of the target MMPs with the highest RMSF value obtained for MMP2. Furthermore, 2D fluctuation plots and

simulation models of target MMPs and the finest interaction pose of target MMPs with the best ligand gave a deeper and very insightful information about the stable interaction and the distinct conformational changes of the amino acid residues on the target MMPs. On further validation of this in silico work, through appropriate in vitro and in vivo research studies, a phytonutraceutical of *Allium ascalonicum*, 1-[[3,5-bis(phenylmethoxy) phenyl]methyl]-6-methoxy-2-methyl-3,4-dihydro-1*H*-isoquinoline can be formulated to a more sustainable drug for treating ovarian cancer at advanced and metastatic stages.

Data availability

" Data will be available from the corresponding author on reasonable request".

Received: 18 November 2024; Accepted: 11 March 2025
Published online: 18 March 2025

References

1. Luo, Z. et al. Tumor microenvironment: the culprit for ovarian cancer metastasis? *Cancer Lett.* **377**(2), 174–182. https://doi.org/10.1016/j.canlet.2016.04.038 (2016).
2. Carey, P., Low, E., Harper, E. & Stack, M. Metalloproteinases in ovarian cancer. *Int. J. Mol. Sci.* **22**(7), 3403. https://doi.org/10.3390/ijms22073403 (2021).
3. López-Otín, C. & Bond, J. Proteases: multifunctional enzymes in life and disease. *J. Biol. Chem.* **283**(45), 30433–30437. https://doi.org/10.1074/jbc.R800035200 (2008).
4. Al-Alem, L. & Curry, T. E. Jr. Ovarian cancer: involvement of the matrix metalloproteinases. *Reproduction* **150**(2), R55–64. https://doi.org/10.1530/REP-14-0546 (2015).
5. Zhang, Y. & Chen, Q. Relationship between matrix metalloproteinases and the occurrence and development of ovarian cancer. *Braz J. Med. Biol. Res.* **50**(6), e6104. https://doi.org/10.1590/1414-431X20176104 (2015).
6. Kenny, H. A., Krausz, T., Yamada, S. D. & Lengyel, E. Use of a novel 3D culture model to elucidate the role of mesothelial cells, fibroblasts and extra-cellular matrices on adhesion and invasion of ovarian cancer cells to the omentum. *Int. J. Cancer.* **121**(7), 1463–1472. https://doi.org/10.1002/ijc.22874 (2007).
7. Klymenko, Y. et al. Cadherin composition and multicellular aggregate invasion in organotypic models of epithelial ovarian cancer intraperitoneal metastasis. *Oncogene* **36**(42), 5840–5851. https://doi.org/10.1038/onc.2017.171 (2017).
8. Lengyel, E. et al. Epithelial ovarian cancer experimental models. *Oncogene* **33**(28), 3619–3633. https://doi.org/10.1038/onc.2013.321 (2014).
9. Fishman, D. A., Bafetti, L. M. & Stack, M. S. Membrane-type matrix metalloproteinase expression and matrix metalloproteinase-2 activation in primary human ovarian epithelial carcinoma cells. *Invasion Metastasis*. **16**(3), 150–159 (1996). https://pubmed.ncbi.nlm.nih.gov/9186550/
10. Moss, N. M. et al. Ovarian cancer cell detachment and multicellular aggregate formation are regulated by membrane type 1 matrix metalloproteinase: a potential role in I.p. Metastatic dissemination. *Cancer Res.* **69**(17), 7121–7129. https://doi.org/10.1158/0008-5472.CAN-08-4151 (2009).
11. Kenny, H. A., Kaur, S., Coussens, L. M. & Lengyel, E. The initial steps of ovarian cancer cell metastasis are mediated by MMP-2 cleavage of vitronectin and fibronectin. *J. Clin. Invest.* **118**(4), 1367–1379. https://doi.org/10.1172/JCI33775 (2008).
12. Kenny, H. A. & Lengyel, E. MMP-2 functions as an early response protein in ovarian cancer metastasis. *Cell. Cycle*. **8**(5), 683–688. https://doi.org/10.4161/cc.8.5.7703 (2009).
13. Lengyel, E. et al. Expression of latent matrix metalloproteinase 9 (MMP-9) predicts survival in advanced ovarian cancer. *Gynecol. Oncol.* **82**(2), 291–298. https://doi.org/10.1006/gyno.2001.6243 (2001).
14. Jabłońska-Trypuć, A., Matejczyk, M. & Rosochacki, S. Matrix metalloproteinases (MMPs), the main extracellular matrix (ECM) enzymes in collagen degradation, as a target for anticancer drugs. *J. Enzyme Inhib. Med. Chem.* **31**(sup1), 177–183. https://doi.org/10.3109/14756366.2016.1161620 (2016).
15. Pahwa, R., Chhabra, J., Kumar, R. & Narang, R. Melphalan: Recent insights on synthetic, analytical and medicinal aspects. *Eur. J. Med. Chem.* **238**, 114494. https://doi.org/10.1016/j.ejmech.2022.114494 (2022).
16. Kühne, A. et al. Population pharmacokinetics of Melphalan and glutathione S-transferase polymorphisms in relation to side effects. *Clin. Pharmacol. Ther.* **83**(5), 749–757. https://doi.org/10.1038/sj.clpt.6100336 (2008).
17. Ravindranath, K. J., Christian, S. D. & Srinivasan, H. Screening of Anti-carcinogenic properties of phytocompounds from allium ascalonicum for treating breast cancer through in Silico and in vitro approaches. *Appl. Biochem. Biotechnol.* **195**(2), 1136–1157. https://doi.org/10.1007/s12010-022-04202-1 (2023).
18. Trott, O. & Olson, A. J. AutoDock Vina: improving the speed and accuracy of Docking with a new scoring function, efficient optimization, and multithreading. *J. Comput. Chem.* **31**(2), 455–461. https://doi.org/10.1002/jcc.21334 (2010).
19. Ravindranath, K. J., Mohaideen, N. S. M. H. & Srinivasan, H. Phytocompounds of onion target heat shock proteins (HSP70s) to control breast cancer malignancy. *Appl. Biochem. Biotechnol.* **194**(10), 4836–4851. https://doi.org/10.1007/s12010-022-04016-1 (2022).
20. Kuriata, A. et al. CABS-flex 2.0: a web server for fast simulations of flexibility of protein structures. *Nucleic Acids Res.* **46**(W1), W338–W343. https://doi.org/10.1093/nar/gky356 (2018).
21. Lemilemu, F., Bitew, M., Demissie, T. B., Eswaramoorthy, R. & Endale, M. Synthesis, antibacterial and antioxidant activities of Thiazole-based schiff base derivatives: a combined experimental and computational study. *BMC Chem.* **15**(1), 67. https://doi.org/10.1186/s13065-021-00791-w (2021).
22. Shen, Z., Yu, M. & Zhang, S. Network pharmacology and molecular docking analyses unveil the mechanisms of Yiguanjian decoction against Parkinson's disease from inner/outer brain perspective. *Biomed. Res. Int.* **2022**, 4758189. https://doi.org/10.1155/2022/4758189 (2022).
23. Katritzky, A. R. et al. Solov'ev V. Skin permeation rate as a function of chemical structure. *J. Med. Chem.* **49**(11), 3305–3314. https://doi.org/10.1021/jm051031d (2006).
24. Kumar, S. A., Mohaideen, N. S. M. H. & Srinivasan, H. Phytocompounds from edible oil seeds target hub genes to control breast cancer. *Appl. Biochem. Biotechnol.* **195**(2), 1231–1254. https://doi.org/10.1007/s12010-022-04224-9 (2023).
25. Phong, N. V. et al. PTP1B Inhibition studies of biological active phloroglucinols from the rhizomes of dryopteris crassirhizoma: kinetic properties and molecular Docking simulation. *Int. J. Biol. Macromol.* **88**, 719–728. https://doi.org/10.1016/j.ijbiomac.2021.08.091 (2021).
26. Wang, Y. et al. Design, synthesis, and biological evaluation of 1-styrenyl isoquinoline derivatives for anti-hepatocellular carcinoma activity and effect on mitochondria. *Eur. J. Med. Chem.* **256**, 115420. https://doi.org/10.1016/j.ejmech.2023.115420 (2023).
27. Zhu, X. et al. Liensinine inhibits progression of intrahepatic cholangiocarcinoma by regulating TGF-β1 /P-smad3 signaling through HIF-1a. *Mol. Carcinog.* **63**(4), 772–784. https://doi.org/10.1002/mc.23687 (2024).
28. Ghauri, M. A. et al. Sanguinarine impedes metastasis and causes inversion of epithelial to mesenchymal transition in breast cancer. *Phytomedicine* **84**, 153500. https://doi.org/10.1016/j.phymed.2021.153500 (2021).

Acknowledgements
The authors are very much grateful to the School of Life Sciences, B. S. Abdur Rahman Crescent Institute of Science and Technology, Chennai, for providing research facilities and also for their unconditional support and encouragement.

Author contributions
HS-Conceptualization, supervision, Editing the manuscript. KJR-Performed experiments, analyzed data and written original version of the manuscript.

Funding
This work was supported by University Grants Commission (UGC), Scheme No. 18, SJSGC 2022-23, New Delhi, India [UGC Award letter Number: F. No. 82 – 7/2022(SA-III) and UGC-Reference Number: UGCES-22-OB-TAM-F-SJSGC-6471].

Declarations

Competing interests
The authors declare no competing interests.

Additional information
Supplementary Information The online version contains supplementary material available at https://doi.org/10.1038/s41598-025-94111-0.

Correspondence and requests for materials should be addressed to H.S.

Reprints and permissions information is available at www.nature.com/reprints.

Publisher's note Springer Nature remains neutral with regard to jurisdictional claims in published maps and institutional affiliations.